Ground vibration induced by high speed trains on an embankment with pile-board foundation

Modelling and validation with in situ tests

Wang, Li; Wang, Ping; Wei, Kai; Dollevoet, Rolf; Li, Zili

DOI
10.1016/j.trgeo.2022.100734

Publication date
2022

Document Version
Final published version

Published in
Transportation Geotechnics

Transportation Geotechnics 34 (2022) 100734

Contents lists available at ScienceDirect

Transportation Geotechnics

journal homepage: www.elsevier.com/locate/trgeo

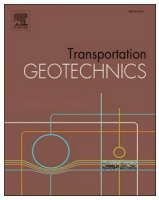

Ground vibration induced by high speed trains on an embankment with pile-board foundation: Modelling and validation with in situ tests

Li Wang [a,b], Ping Wang [b], Kai Wei [b,*], Rolf Dollevoet [a], Zili Li [a,*]

[a] Section of Railway Engineering, Delft University of Technology, Stevinweg 1, 2628CN Delft, the Netherlands
[b] Key Laboratory of High-speed Railway Engineering (Southwest Jiaotong University), Ministry of Education, Chengdu 610031, China

ARTICLE INFO

Keywords:
Ground vibration
High speed railway
Soft soil
Pile-board structure
Finite element model
Local vibration amplification

ABSTRACT

To investigate the train-induced ground vibration, an explicit time-domain, three dimensional (3D) finite element (FE) model is developed. The train, track, embankment, pile-board structure and nearby ground soils are all fully coupled in this model. The complex geometries involving the track components and pile-board structure are all modelled in detail, which makes the simulation of wave propagation more realistic from the train to the ground. The model is validated with in situ tests data collected in the Beijing-Shanghai high speed railway line. Good agreements have been achieved between the numerical results and experimental results both in time domain and frequency domain. The proposed model is thus capable of reproducing the dynamic ground response induced by a typical high speed train. Soil responses induced by different number of vehicles are compared. With more vehicles, the spectral peaks of soil responses are more prominent at the integral multiples of the vehicle passing frequency. Too few vehicles will not bring about such phenomenon, thus sufficient number of vehicles should be included in a train to properly model train-induced ground vibration. With the proposed model, the influence of the pile-board foundation on the ground vibration is investigated. It is found that the pile-board foundation can significantly attenuate the low frequency ground vibration. The attenuation of the ground vibration as a function of distance from the track is simulated and the influential factors to the local vibration amplification are investigated. It is found that soil Young's modulus and soil impedance contrast are the two main factors influential to the local vibration amplification. The softer the natural soil, the larger the amplification. The larger soil impedance contrast makes the amplification more obvious. The soil stratification and geometric discontinuity at ground surface are not the main cause of the local vibration amplification in this work.

Introduction

Rail transport is extensively adopted all over the world because of its cost-effectiveness and energy efficiency. Yet the train-track dynamic interaction induces vibration, causing environment problems. Especially, excessive ground vibration induced by high speed trains or subways may be nuisance to nearby residents, may cause malfunctioning of sensitive equipment in hospitals and laboratories, and in extreme cases may even cause damage to historical sites and buildings [1–3]. The train-induced ground vibration is of growing concern in the past thirty years because of the fast development of intercity and urban rail transport [4–7].

To predict the influences of ground vibration, analytical, semi-analytical or 2D numerical models were used to investigate the surface waves induced by moving train loads [8–13]. These models were very useful and efficient to find the key parameters involved in the phenomenon of ground vibration. Yet, limitations in considerations of complex geometries and materials make them having difficulties in simulating some real scenarios.

Afterwards, finite element (FE) method was introduced with its advantages in dealing with the irregularities in geometry and material nonlinearities, including natural soil layers and embedded structures. However, applications were usually limited to 2D models because using full 3D formulations was almost impossible from a computational point of view at early times.

As an alternative to time-domain full 3D FE models, the 2.5D approach was proposed for the prediction of railway induced vibrations. Yang and Huang [14] developed a 2.5D finite/infinite element procedure, and Yang, *et al.* [15] used this procedure to study the train-induced wave propagation in layered soils. Jean, *et al.* [16] presented a 2.5D

* Corresponding authors.
E-mail addresses: weimike@home.swjtu.edu.cn (K. Wei), z.li@tudelft.nl (Z. Li).

https://doi.org/10.1016/j.trgeo.2022.100734
Received 12 October 2021; Received in revised form 25 January 2022; Accepted 25 January 2022
Available online 29 January 2022

Fig. 1. The test site.

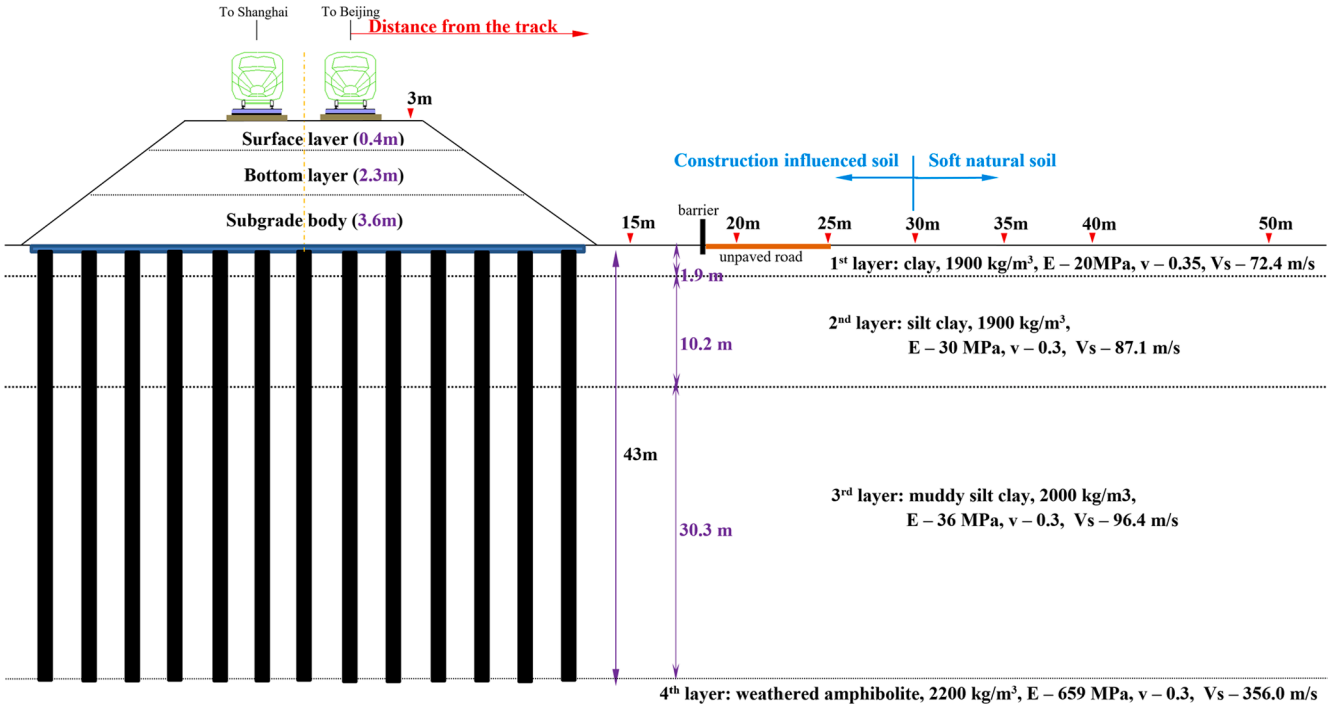

Fig. 2. Schematic diagram of the cross section and measurement points at various distances from the track (E – Young's modulus, v – Poisson's ratio, Vs – shear wave velocity).

model using a full boundary element (BE) method to study ground structure interaction due to surface waves. Sheng, *et al.* [17,18] established a 2.5D finite element–boundary element (FE-BE) model to investigate the ground vibration caused by the railway traffic on the ground and in a tunnel. To account for the periodicity appearing in the track direction, such as rail supports, track slabs and tunnel segments, Degrande *et al.* [19] developed a 3D periodic FE-BE approach to predict the free field response due to metro trains in tunnels. Gupta, *et al.* [20] used the periodic FE-BE approach to study the vibrations caused by the passage of a Thalys high speed train in the Groene Hart tunnel. In general, the 2.5D approach and the 3D periodic FE-BE approach need to consider only the profile perpendicular to the train's moving direction and assumes the geometries and material properties to be constant or periodic along the train's moving direction. This makes these methods efficient when involving complex geometries and material properties. It also limits their applications to situations where it is reasonable to assume such invariance or periodicity in train's moving direction.

With the rapid development of computational power, 3D time-domain method becomes more attractive for simulating train-induced ground vibration. Ju and Lin [21] developed a 3D FE model to analyse the isolation effects of concrete slab and soil improvement. Galvin, *et al.* [22] established a 3D time-domain multi-body-FE-BE model to analyse

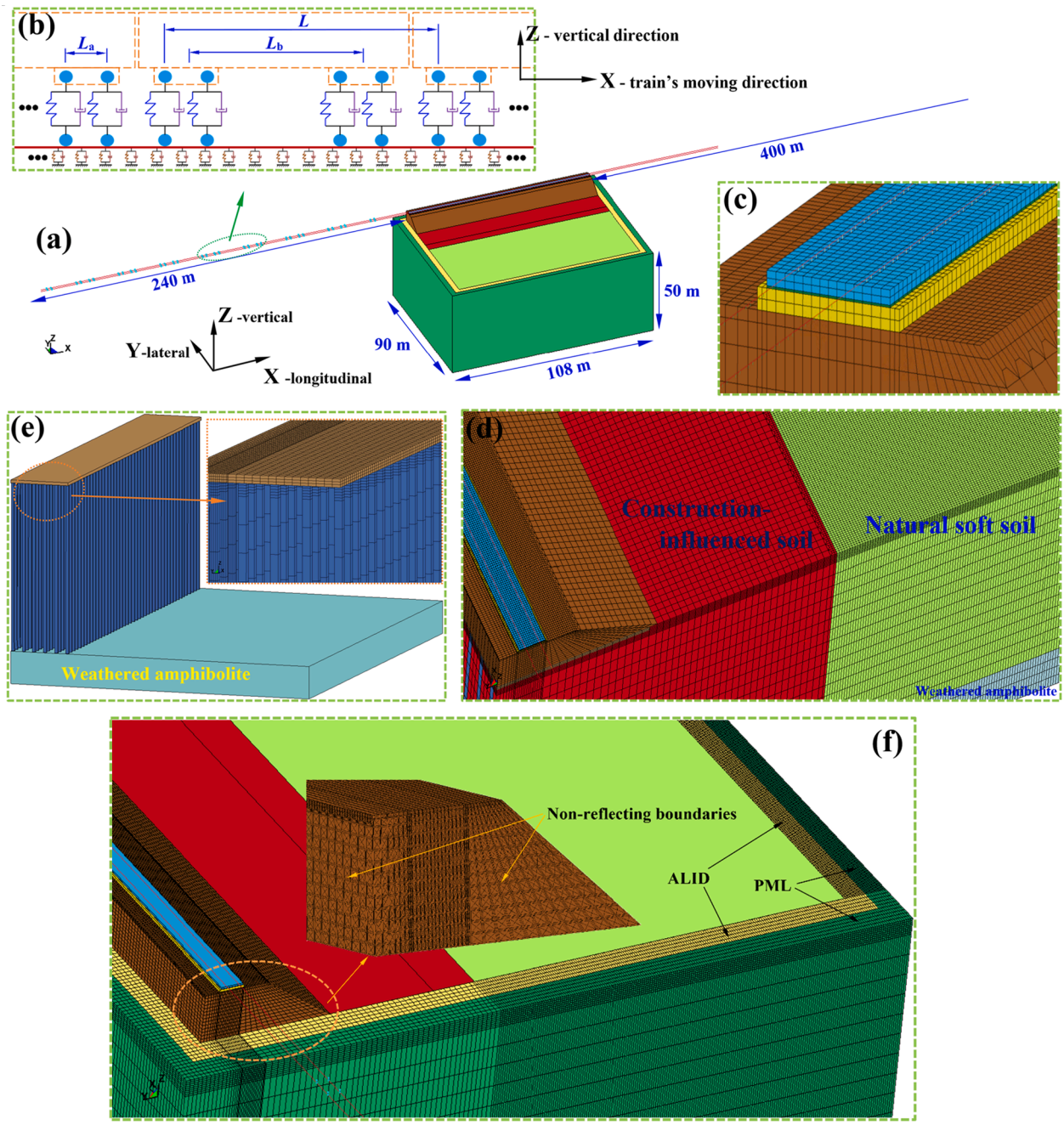

Fig. 3. Fully coupled 3D train-track-piles-soil FE model: (a) dimensions; (b) train model; (c) track structure and its mesh; (d) embankment and ground soils mesh; (e) pile-board structure and its mesh; (f) perfectly matched layer (PML), absorbing layers by increasing damping (ALID) and non-reflecting boundaries.

the dynamic behaviour of a transition zone between a ballasted track and a slab track. Kouroussis, *et al.* [23] developed a compound vehicle-track-soil model which contains two subsystems: vehicle-track subsystem and soil subsystem. The vehicle-track subsystem allows for a detailed vehicle model with the help of a multi-body approach. This 3D time-domain model was used to investigate the influences of some vehicle and track parameters, as well as soil properties on the ground vibration [24,25]. Connolly, *et al.* [26] updated this model to be a more coupled 3D FE model with an elongated spherical domain to achieve improved absorption performance of reflected waves at the soil boundaries. To consider the real scenario of high speed railway on pile-reinforced soft soils, Li, *et al.* [27,28] developed a fully coupled 3D vehicle-track-pile-soil model to investigate the influences of piles on the ground vibration responses in high-speed railway with slab tracks. Overall, good agreement has been achieved when comparing numerical results with field test results in terms of peak particle accelerations. The model considered only one vehicle and the analysis did not include the responses induced by multiple vehicles of a train, particularly the responses in frequency domain.

To understand the characteristics of ground vibration induced by high speed trains on embankment, many in situ experiments have been performed. Degrande and Schillemans [4] measured the free field vibrations and track responses induced by the Thalys high speed trains with speed varying from 223 to 314 km/h. Auersch [29] presented three series of measurements during the test runs of ICE on a newly built track in Germany and the test data was used in the validation of an integrated model. In China, at the Beijing-Shanghai high speed line, Zhai, *et al.* [30] performed a field measurement of ground vibration with train speed up to 410 km/h. Feng, *et al.* [31] conducted ground vibration measurements considering different sections with embankment, culvert, viaduct

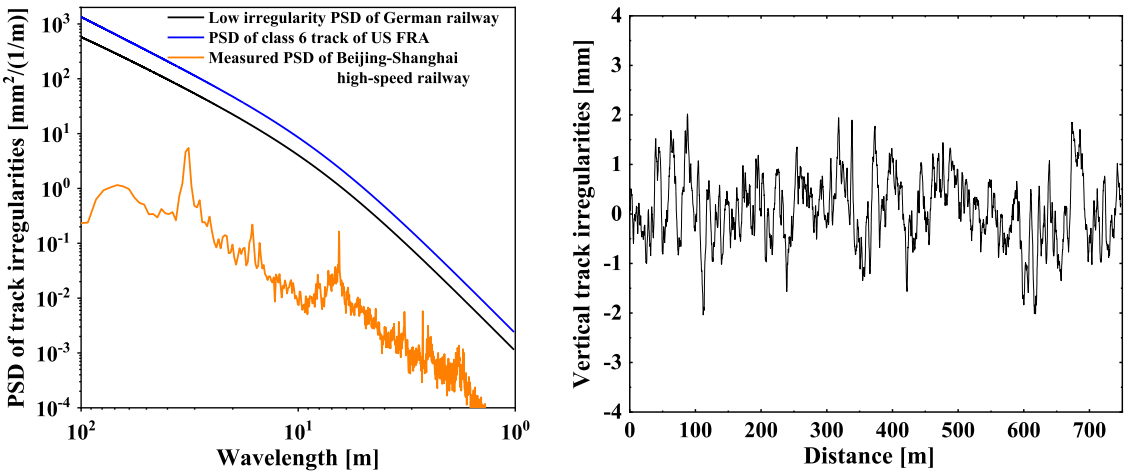

(a) Measured irregularities power spectra density [32, 35 - 38] (b) Space domain irregularities profile used in simulations

Fig. 4. Vertical track irregularities at the test site.

Table 1
Parameters of vehicle.

	Mass [kg]	Stiffness [N/m]	Damping [N.s/m]
Carbody	38,884	/	/
Bogie	3060	/	/
Wheelset	1517	/	/
Primary suspension	/	1.772E6	2E4

and transition zones, respectively. In the authors' previous work [32], the frequency-domain characteristics of the ground vibration caused by high-speed trains are experimentally studied. The in situ measurements are valuable for providing data sets in the validation of numerical models.

In the present work, an explicit time-domain, fully coupled 3D dynamic train-track-embankment-piles-soil model is developed and validated with in situ tests both in time domain and frequency domain. The paper is organized as follows. Section 2 briefly introduces the experimental campaign in the authors' previous work [32]. Section 3 presents the detailed modelling approach. Section 4 is the validation of the proposed model. In Section 5, the soil responses with various number of vehicles are investigated, the ground vibrations with and without the pile-board foundation are compared, and the influential factors to the local vibration amplification are discussed. Finally, Section 6 presents the conclusions and future work.

Experimental campaign

This section introduces the experimental campaign in brief, the test results from which are used to validate the 3D FE model in Section 3. More information about the experimental campaign can be found in [32].

Overview of the test site

An experimental campaign was conducted at Kunshan, Jiangsu province in China, along the high speed railway line between Beijing and Shanghai. The test site is in a soft soil region in the Yangtze delta, where the soil modulus could be as low as only several mega Pascal. To support the high speed trains in such a soft soil region, pile-board composite foundation is adopted. Above the reinforced foundation, the test site consists of two slab tracks on an embankment which is about 6 m in thickness. The test site is shown in Fig. 1. Alongside the embankment, there is a concrete barrier/fence, an unpaved road and a shallow trench.

High speed train traffic

The high-speed trains running on the track were the CRH380 series, including 8-carriage CRH380A and CRH380B, as well as 16-carriage CRH380AL and CRH380BL. A 16-carriage CRH380AL is a combination of two 8-carriage CRH380A, so as to the relationship between CRH380BL and CRH380B. The configurations of all the carriages are

Table 3
Parameters of fasteners.

	Stiffness [N/m]	Damping [N•s/m]
At the main part	2.5E7	7.5E4
At the approaching and leaving parts	*1.2E7*	*7.5E4*

Table 2
Parameters of the track and substructures.

		Elastic modulus [Pa]	Poisson's ratio	Density [kg/m^3]	Rayleigh damping	
					α [s^{-1}]	β [s]
Rail		2.06E11	0.3	7800	/	/
Track slab		3.45E10	0.2	2400	*0*	*0.0001*
CA mortar		7.0E9	0.2	1900	*0*	*0.0005*
Base plate		3.25E10	0.2	2200	*0*	*0.0001*
Embankment		*1.5E8*	*0.2*	*2000*	*0*	*0.01*
Pile-board		3.0E10	0.2	2200	*0*	*0.0001*
Ground soils	*Construction-influenced soil*	*90E6*	*0.3*	*2000*	*0.02*	*0.08*
	Natural soft soil	*10E6*	*0.3*	*1600*	*1.257*	*0.01*
	Weathered amphibolite	*700E6*	*0.3*	*2000*	*0*	*0.001*

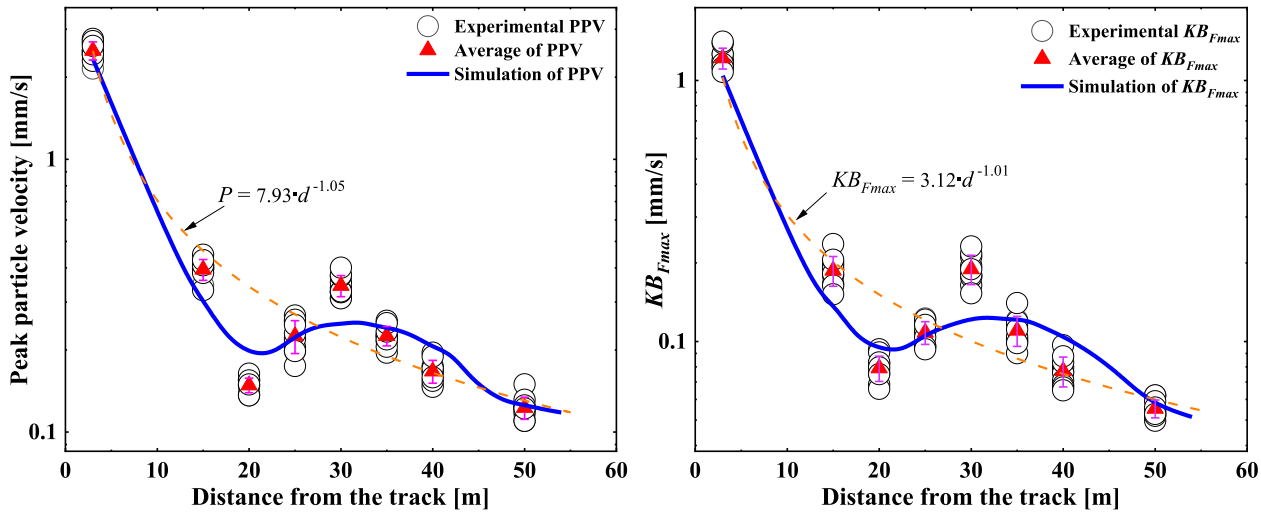

Fig. 5. Soil surface vibration as the increase of distance from the track: (a) PPV; (b) KB_{Fmax}. (At each measurement location, there are 10 circles and each circle represents one train passage. The pink error bar along with the average value at each location is the standard deviation of the measurement data).

similar. The length of each vehicle is about 25 m and the wheelbase of each bogie is 2.5 m. The static axle load is about 140 kN and the train operating speed is about 250 km/h or 300 km/h. During the test, 10 train passages were recorded with speed varying from 296 km/h to 307 km/h. Of the 10 train passages, there were 8 16-carriage trains and 2 8-carriage trains.

Track structure, embankment and substructure

The track structure at the test section is the Chinese railway type II (CRTS II) slab track which consists of rail (60 kg/m), fastener, track slab, cement asphalt (CA) mortar and base plate. The track slabs and the base plates are all anchored longitudinally.

The embankment is composed of 3 layers: surface layer, bottom layer and subgrade bed. The surface layer is filled with graded crush stones with a thickness of 0.4 m. The bottom layer and the subgrade bed are filled with special designed group fillers [33].

The pile-board composite foundation below the embankment has piles of 43 m long with a diameter of 0.5 m. The space between every two piles is 2.4 m.

The embankment and pile-board structure are shown in Fig. 2.

Ground soils and soil response measurements

The soft soil at the location consists of multi-layered clay and silt clay with elastic modulus as low as 20 MPa. More information about the soil properties can be found in [32]. The vertical vibration velocities of the soil surface are recorded at 8 locations, i.e., 3, 15, 20, 25, 30, 35, 40 and 50 m away from the track centre, as shown in Fig. 2. The point at 3 m is on the shoulder of the embankment, and the points at 20 and 25 m are on the unpaved road. From about 30 m away from the track, the ground is full of soft natural soil without much disturbance, while at the places close to the embankment, the ground soil could have been influenced by the construction before, such as pile-driving. In addition, the soil properties in Fig. 2 were acquired from a borehole about 150 m away from the test location. The actual soil properties at the test location could be locally different. Therefore, the soil properties in Fig. 2 mainly serve as references in this modelling.

Modelling approach

Model overview

The main part of the model, with the structure of Fig. 2, is 108 m in the train's moving direction, as shown in Fig. 3(a). The two rails of a track are extended with simplified supports at the two ends of the main part in order to properly consider the effects of the trains when they approach and leave the main part, while limiting the overall model within reasonable size to be computationally efficient. At the approaching end, the rails are extended 240 m so that a train of 200 m long (CRH380A or CRH380B) can run from there onto the main part. At the leaving end, the rails are extended 400 m in order to allow the train to run for a sufficiently long time so that the train-induced vibration and wave phenomena can be fully developed in the main part. Thus, the model is in total 748 m long. The train speed can be defined to simulate accelerating, steady-state moving and braking. The double-track Beijing-Shanghai high speed line is symmetrical in the train's moving direction, thus only one track and half embankment, as well as half foundation and half supporting soil layers are modelled, as shown in Fig. 3 (a).

Train modelling

In the train modelling, the train consists of 8 vehicles. For each vehicle, the carbody, two bogies and the secondary suspensions are together lumped into 8 equal mass points. The 8 wheels are lumped into 8 mass points accordingly. The primary suspensions are modelled as springs and dampers connecting the 8 pairs of mass points, as shown in Fig. 3(b).

The displacements of the mass points are constrained in the lateral direction (Y-direction, as shown in Fig. 3(a)). In the longitudinal direction (X-direction, i.e., train's moving direction), all the mass points are coupled together traveling with the same longitudinal train speed, and no relative longitudinal movement is allowed between the mass points. In the vertical direction (Z-direction), there is no special constraint on the mass points. The vehicle length L, bogie spacing L_b and axle spacing L_a are 25 m, 17.5 m and 2.5 m, respectively.

Track structure and wheel-rail contact

The two rails are modelled with beam elements. The fasteners are

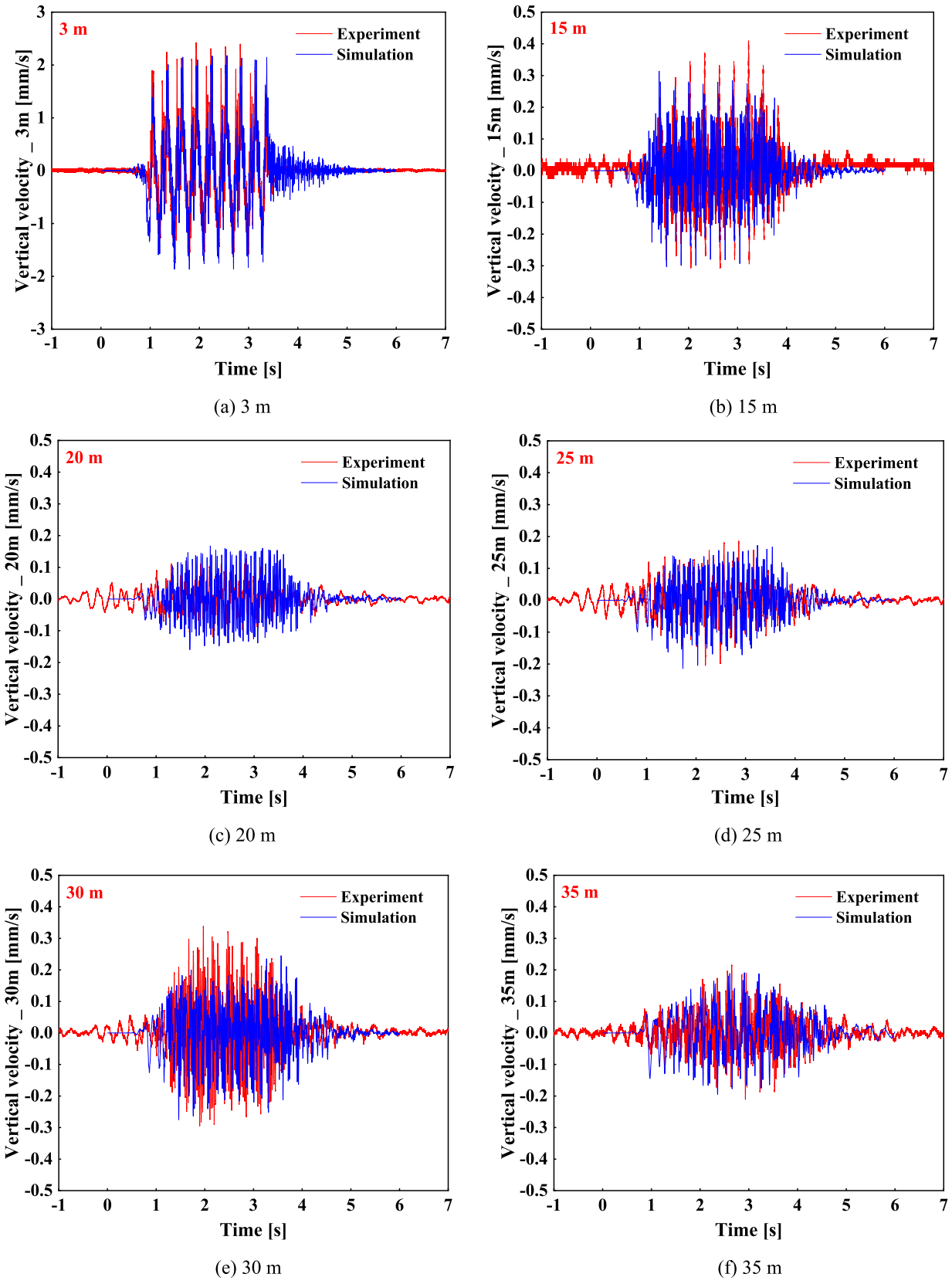

Fig. 6. Measured and simulated history of vertical velocities at various locations during the passage of an 8-carriage high-speed train at the speed of 300 km/h.

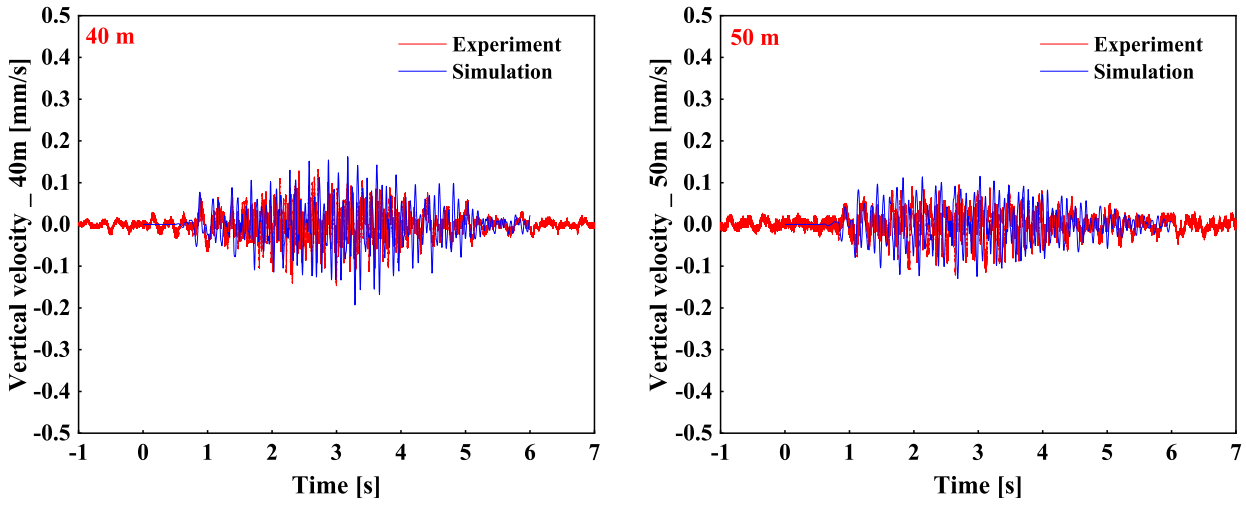

(g) 40 m (h) 50 m

Fig. 6. (*continued*).

modelled as springs and dampers. The parameters of the fasteners of the main part are as determined in [32]. For the fasteners at the approaching and leaving parts, the parameters are obtained by trial simulations to ensure that their rail deflections are at the same level as that of the main part to avoid unphysical disturbances at the transitions between the main part and the extended parts. The other components, namely, the slab, CA mortar layer and the base plate are all modelled with 8-node solid elements, as shown in Fig. 3(c).

The wheel-rail contact is defined as the wheel mass points moving along the rails. The vertical contact force F is

$$F = K_{\mathrm{h}} \cdot (Z_{\mathrm{w}} - Z_{\mathrm{r}} - \delta) \tag{1}$$

where K_{h} is the contact stiffness, Z_{w} is the displacement of wheel, Z_{r} is the displacement of rail, and δ is the input track geometry irregularities. A linear contact stiffness of 1.32E9 N/m is assumed [28,34], while no tensile force is generated when the wheel loses contact with the rail.

The vertical track geometry was measured over 18 km around the test site. Its power spectrum density (PSD) is shown in Fig. 4(a). Shown are also the spectra of the German railway and of the class 6 track of the US FRA for comparison [35–37]. The track irregularities shown in Fig. 4 (b) were derived from the measured PSD according to [38] and they were input to the model.

Embankment, pile-board structure and ground soils modelling

The embankment, pile-board and ground soils are all modelled with 8-node 3D solid elements, as shown in Fig. 3(d) and (e). Because there is no measurement data available in each layer of the embankment, the 3 layers of the embankment have to be treated together in this simulation to avoid identifying the mechanical properties of each layer.

The ground soils consist of 3 parts in this modelling: the weathered amphibolite layer at the bottom, the construction-influenced soil part and the natural soft soil part, as shown in Fig. 3(d). For the natural soft soil part, the surface layer (1.9 m in depth) is in fine mesh with dimensions of 0.2 m × 0.25 m × 0.25 m.

The 43-meter piles are plugged into the weathered amphibolite layer. The pile-board elements share nodes with their surrounding soil elements at their interfaces. Thus at their interfaces, the pile-board foundation and its surrounding soils have no relative displacement. In this coupling way, the pile-board foundation is able to transfer the dynamic train load into the surrounding soil. Friction force between the pile-board foundation and the surrounding soils is included in the forces at the shared nodes. Possible small relative slip between the pile-board and the surrounding soils is ignored. Thus, at the interfaces, static friction is considered instead of kinetic friction. More complex pile-soil interaction will be explored in the future [39].

Boundary considerations

To simulate the wave propagation in an unbounded ground with the truncate soils in this model, perfectly-matched layers (PML) [40] and an approach of absorbing layers by increasing damping (ALID) [41] are used at the model boundaries to avoid wave reflection by absorbing outward waves, as shown in Fig. 3(f). Also, at the boundaries of the embankment, the non-reflecting boundaries are used. These measures ensure the absence of the spurious wave refection [23,28,42]. The boundaries of the perfectly-matched layers are fully constrained.

Computational implementation

The simulations are performed using the commercial FEM software ANSYS/LS-DYNA. In total, there are 3,808,376 elements and 3,984,126 nodes. The time step is fixed at 1.22E-5 s. The calculation time for each case takes about 61 h by a workstation with 12-core processors.

Validation with in situ experiment data

In this section, the model proposed in Section 3 is validated with the in situ tests data. With proper parameters, the proposed model should be capable of reproducing the measured responses induced by passing trains. In this work, the parameters of vehicle, track, and pile-board structure are obtained from references [30,32], as listed in Table 1, Table 2 and Table 3. The parameters of embankment and ground soils, as well as fasteners at approaching and leaving parts, as listed in italic in Tables 2 and 3, are obtained by trial simulations after decent agreements have been reached when comparing numerical results and experimental results.

Parameters obtained by trial simulations

The parameters of the vehicle are listed in Table 1 [30].

The track slab, CA mortar, base plate, embankment and the ground soils are all modelled with linear elastic materials. The parameters of the track and substructures are listed in Table 2 [32].

The classical Rayleigh damping method is applied for all the components with solid elements in this modelling. The damping matrix $\boldsymbol{C}$ is

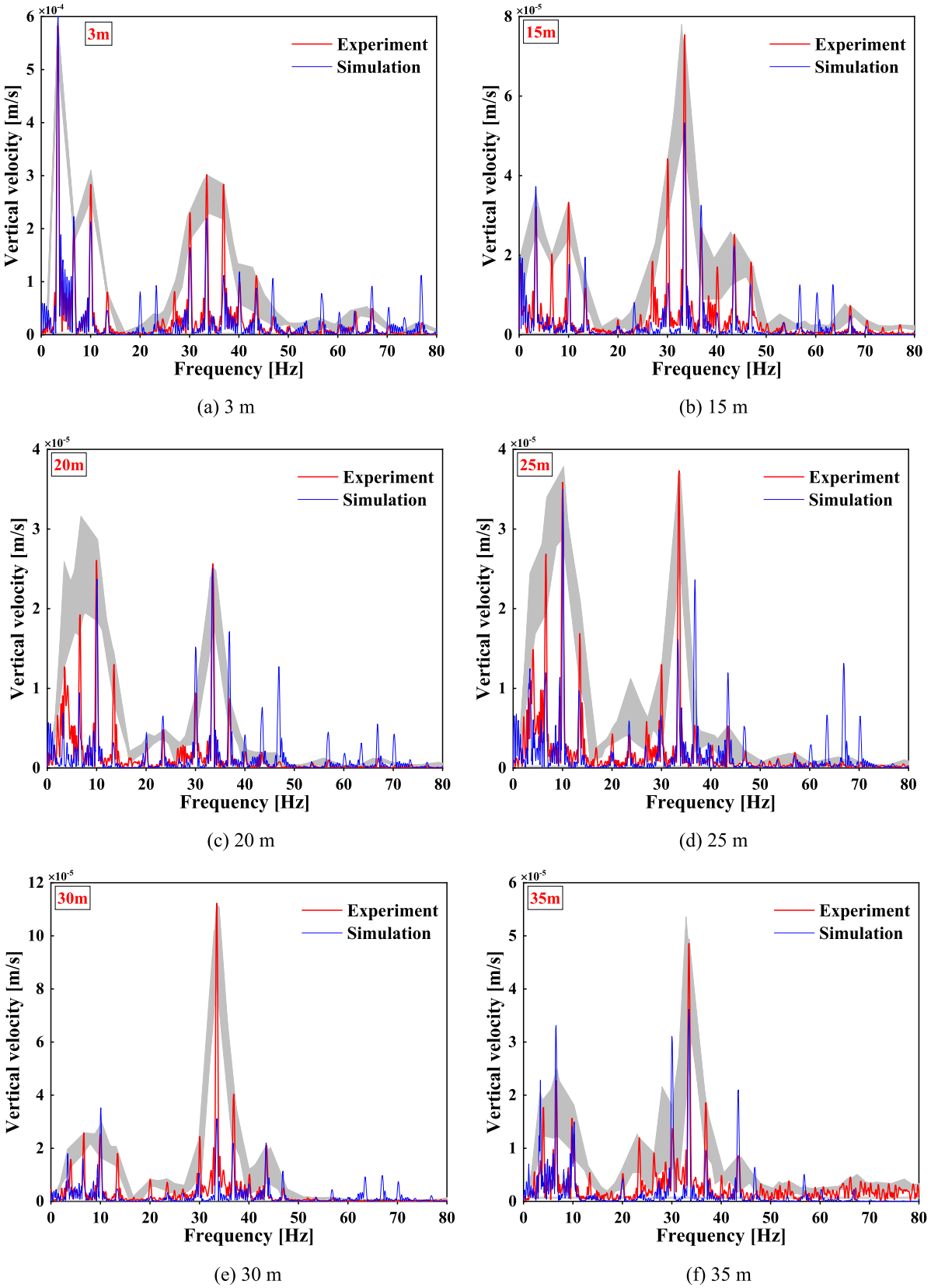

Fig. 7. Measured and simulated vertical velocities in frequency domain at various locations with the train speed of 300 km/h (Grey band is the combination of the outlines of the spectral peaks of all the measured 10 passages).

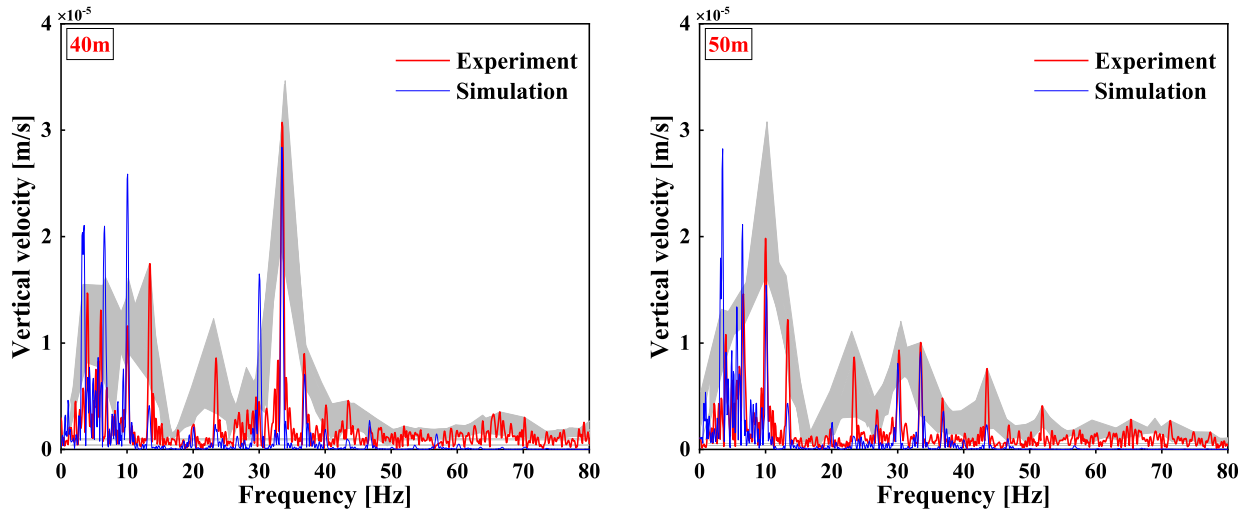

(g) 40 m (h) 50 m

Fig. 7. (*continued*).

given as a linear combination of mass matrix $\boldsymbol{M}$ and stiffness matrix $\boldsymbol{K}$:

$$\boldsymbol{C} = \alpha\boldsymbol{M} + \beta\boldsymbol{K} \tag{2}$$

where α and β are constants of proportionality.

The constants of proportionality for each component in this model are obtained by trial simulations, as listed in italic in Table 2.

As mentioned above, the properties of the fasteners at the approaching and leaving parts are different from that of the fasteners at the main part. The parameters of fasteners are listed in Table 3 [32]. Moreover, in different cases, the properties of the fasteners at the approaching and leaving parts are adjusted accordingly to make sure that there is no unphysical disturbances introduced at the two transitions.

Comparison of experimental and numerical results

PPV and KB_{Fmax}

The peak particle velocity (PPV) and the weighted vibration severity $KB_F(t)$ are two usual indicators to access the effect of vibration [1,23,43]. PPV is defined as the maximum absolute amplitude of the velocity time signal:

$$\mathrm{PPV} = \max|v(t)| \tag{3}$$

Weighted vibration severity $KB_F(t)$ is the time-averaged signal (running root mean square) of $KB(t)$, defined as:

$$KB_F(t) = \sqrt{\frac{1}{\tau}\int_0^t KB^2(\xi)e^{-(t-\xi)/\tau}d\xi} \tag{4}$$

where the time constant τ is 0.125 s, and the weighted velocity signal $KB(t)$ is obtained by passing the original velocity signal through the high-pass filter:

$$|H_{KB}(f)| = \frac{1}{\sqrt{1+(f_0/f)^2}} \tag{5}$$

where the cut-off frequency f_0 is 5.6 Hz. The maximum absolute amplitude $KB_F(t)$ is denoted as KB_{Fmax}:

$$KB_{Fmax} = \max|KB_F(t)| \tag{6}$$

The PPVs and the KB_{Fmax} of the soil surface vibration at the 8 measurement locations are presented in Fig. 5 for the 10 train passages passing at around 300 km/h.

It can be seen from Fig. 5(a) that the measured vertical PPVs generally decrease as a function of the distance from the track. This attenuation was usually fitted with exponential decay functions [1,23] or polynomial equations [31]. The orange dash line is an example of the fitting with an exponential decay function. Yet, at the place about 30 m (25 ~ 40 m) away from the track, as shown in Fig. 5(a), there is an obvious rebound in these measurements. This phenomenon of local vibration amplification was also observed in the measurements in [31] and [44]. In [31], the measurements were also conducted at a site along the Beijing-Shanghai high speed railway line, while in [44], the measurements were performed in a normal railway with train speed from 20 to 80 km/h. The local vibration amplification will be further discussed in Section 5.3. Fig. 5(b) presents the measured KB_{Fmax} changing as a function of the distance from the track. The attenuation of the KB_{Fmax} as the increase of distance is quite similar to that of the PPV.

With the model in Section 3 and the parameters in Section 4.1, both the attenuation of PPV and that of KB_{Fmax} as the increase of distance from the track are successfully simulated, as shown with the blue solid lines in Fig. 5. The rebounds are also reproduced for the two different indicators, even though not perfectly.

Comparison in time domain

It is observed that the measured surface vertical velocities are similar for all the 10 train passages, no matter the train consists of 16 carriages or 8 carriages. This similarity will be shown in Figs. 7 and 8. Thus, a typical 8-carriage CRH380A with measured PPVs close to the average values (see Fig. 5(a)) is chosen for comparison since in our FE model, the train consists of 8 vehicles.

Fig. 6 presents the comparison of the experimental and numerical vertical velocities at the 8 locations in time domain.

It can be seen from Fig. 6 that the numerical results correspond closely to the experimental results, both in magnitude and shape. At the embankment shoulder (3 m away from the track), the response to the passing of each wheelset is visible, and the numerical result and the experimental result match each other well, as shown in Fig. 6(a). At the other places, except the places of 20 m and 30 m, the numerical results match generally well with the experimental results. At the measurement point of 20 m, the experimental result is overestimated in the simulation. It is possibly because the barrier/fence and unpaved road are not well considered in this simulation. At the measurement point of 30 m, the numerical result is a bit smaller than the experimental result in

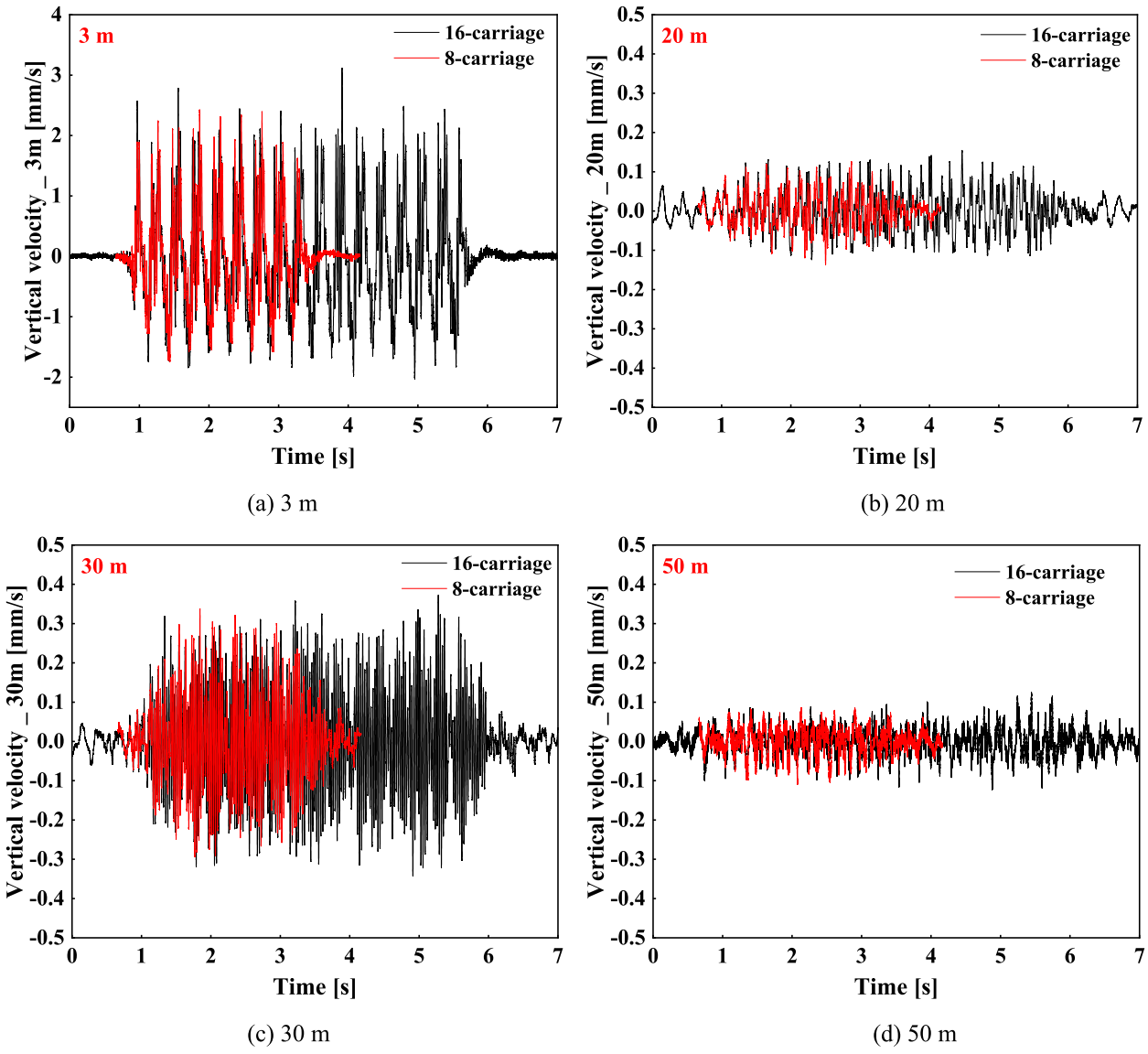

Fig. 8. Soil responses histories at various locations of a typical 16-carriage train and an typical 8-carriage train with train speed both at 300 km/h. (a) 3 m; (b) 20 m; (c) 30 m; (d) 50 m.

magnitude, thus this simulation underestimates the vibration rebound at the place of 30 m from the track. The reasons to this local vibration amplification will be discussed in Section 5.3.

Comparison of frequency contents

Fig. 7 shows the comparison in frequency domain.

It can be seen in Fig. 7 that, at each measurement point, the vibration is usually below 50 Hz. The content above 50 Hz is relatively weak. At the place close to the track (3 m), there are still some responses in the range of 50–80 Hz, while when the distance from the track is 15 m or farther, the high frequency content of 50–80 Hz is almost gone due to the effect of soil damping.

Another frequency-domain characteristic of the measurements is that the spectral peaks are all at the integral multiples of the vehicle passing frequency, namely:

$$f = \mathrm{n}V/L \tag{7}$$

where V is the train speed, L is the vehicle length, n = 1,2,3,…

The amplitudes of the spectral peaks vary to a limited extent for the measured 10 passages, as shown with the narrow grey bands in Fig. 7. Therefore, it is concluded that all the measurements of the 10 passages have similar frequency-domain responses. The frequency-domain soil responses induced by a 16-carriage train are quite close to those induced by an 8-carriage train.

These findings from analysing the ground vertical velocities are consistent with the results of [32] where the measured ground vertical accelerations were analysed.

From Fig. 7, it can be seen that, in general, the spectral peaks in the experimental results are well reproduced in the numerical results. The differences between the numerical results and experimental results are mainly in the relative amplitudes of the spectral peaks. As reported in [45,46] where the measurement points are on the sleepers, the relative amplitudes of the spectral peaks are determined mainly by the train geometry and the relative amplitudes of the wheel loads, as well as the track structures. In this experiment, the measurement points are on soil surface, the soil properties can also influence the relative amplitudes of the spectral peaks. In the experiments, the wheel loads could vary because of the uneven carriage weight distribution and the different out-of-roundness of each wheel. But the influence of different wheel loads in this experiment should be very limited because the 10 passages have close amplitudes of spectral peaks (see the grey bands in Fig. 7). Thus,

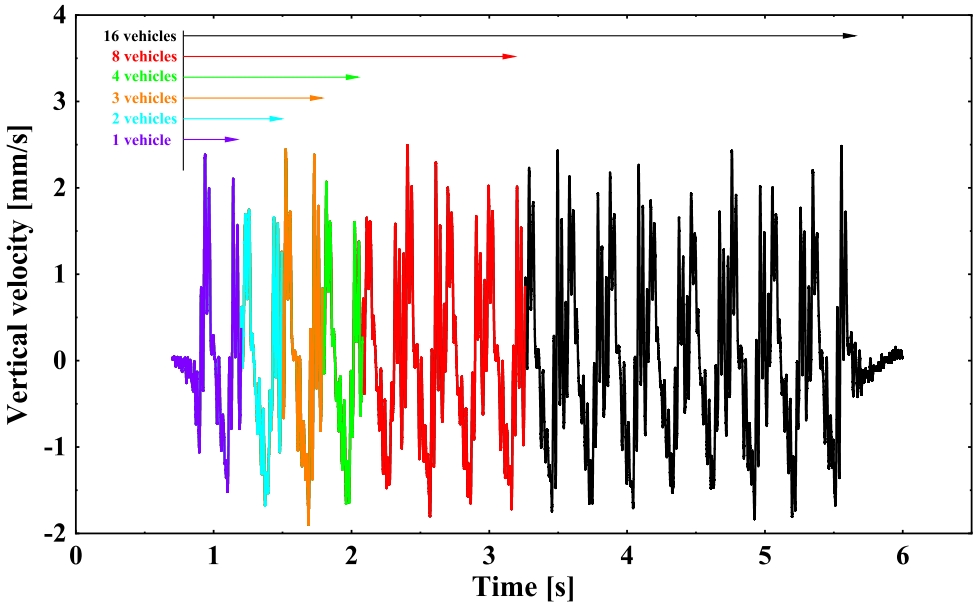

(a) time domain

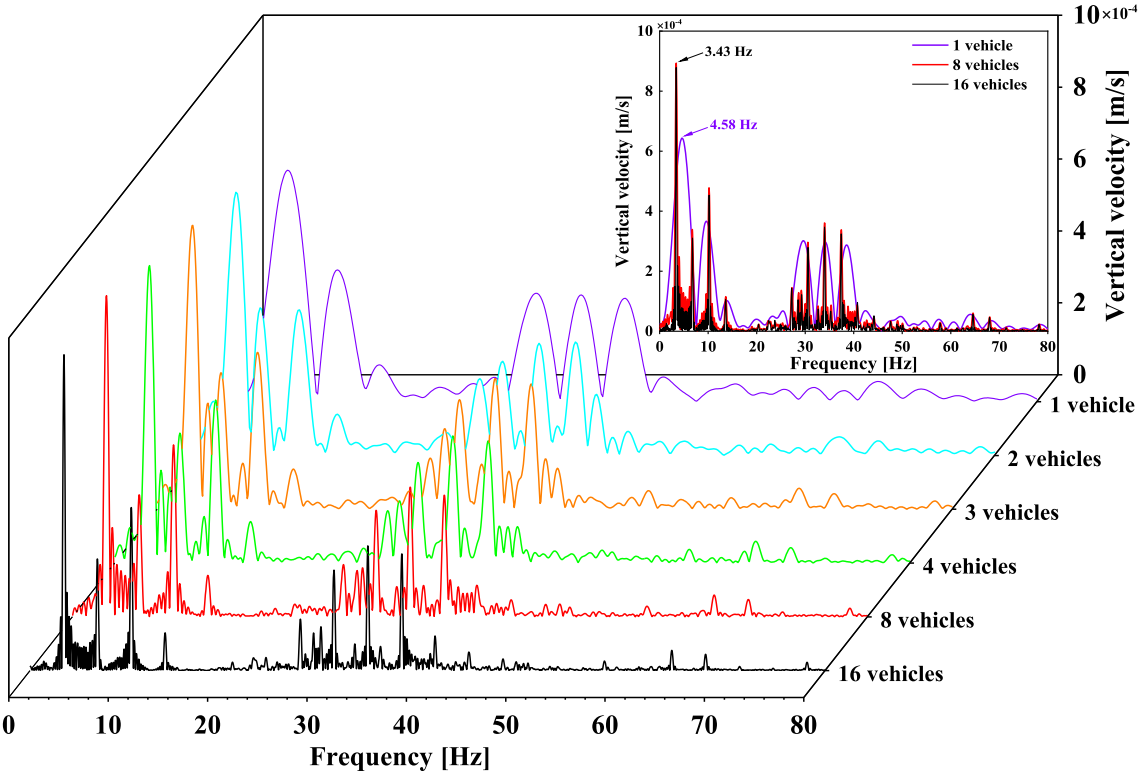

(b) frequency domain

Fig. 9. Soil responses at 3 m with various number of vehicles. (a) in time domain; (b) in frequency domain.

the differences in terms of the relative amplitudes of spectral peaks between the numerical results and experimental results should probably mainly be attributed to the soil properties. The influence of soil properties on the relative amplitudes of spectral peaks will be investigated in the future.

With the observations from in Figs. 6 and 7, it can be concluded that the proposed model can simulate the ground vibrations induced by a typical high speed train.

Discussions

Soil responses with different number of vehicles

In this in situ experiment, a 16-carriage train is two 8-carriage trains coupled with each other. In frequency domain, the16-carriage trains have quite similar soil responses to those of 8-carriage trains, as shown with the grey bands in Fig. 7. They also have similar responses in time domain, as shown in Fig. 8 below.

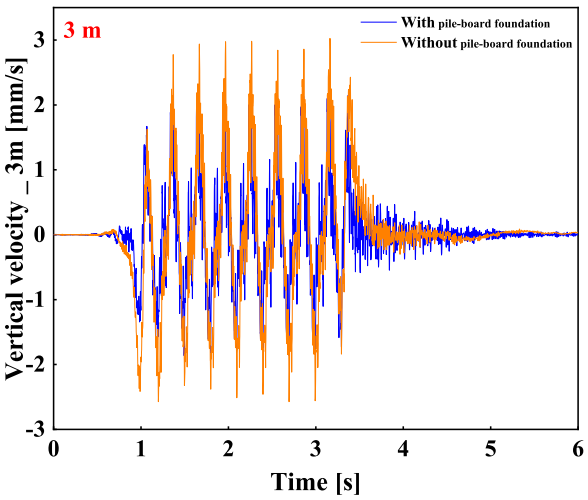

(a) 3 m in time domain

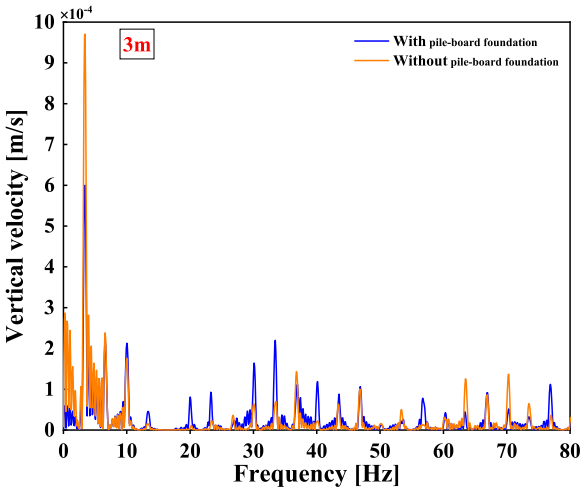

(b) 3 m in frequency domain

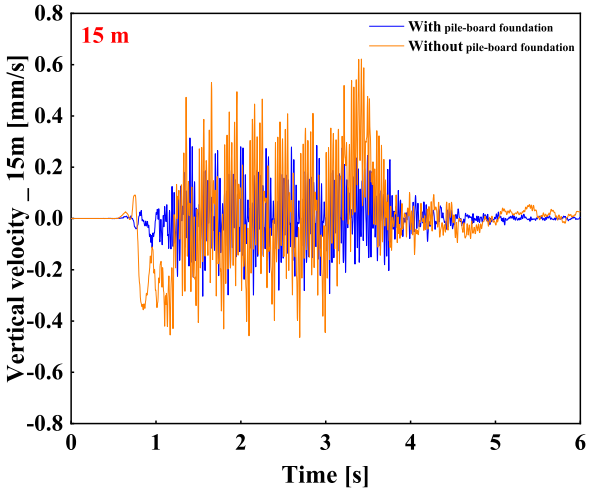

(c) 15 m in time domain

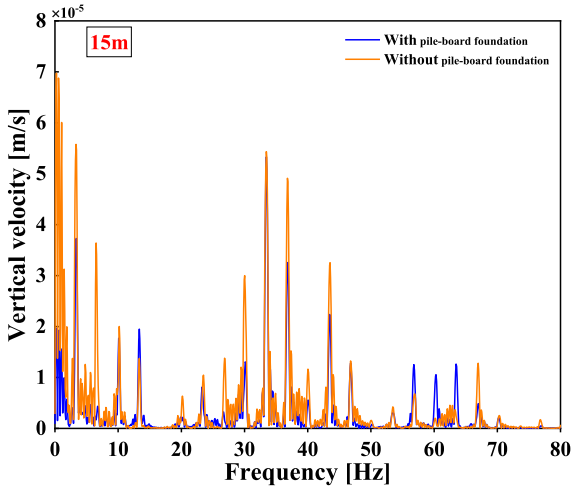

(d) 15 m in frequency domain

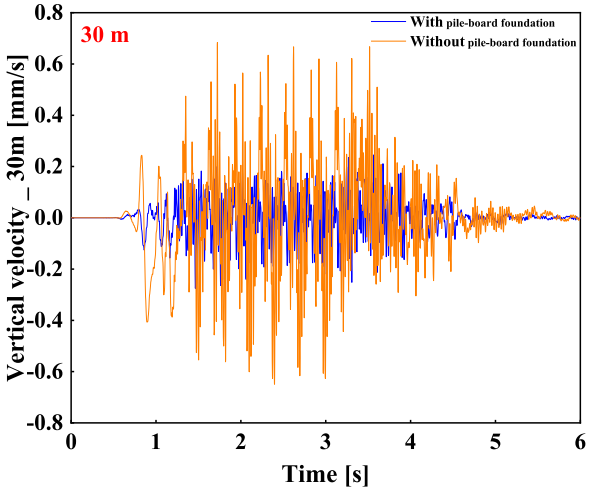

(e) 30 m in time domain

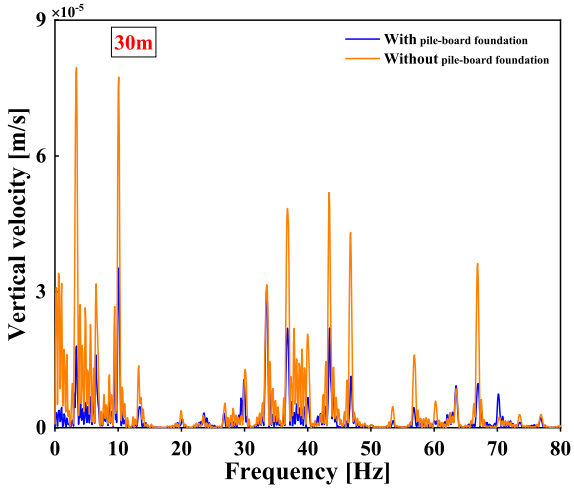

(f) 30 m in frequency domain

Fig. 10. Simulation results with or without pile-board foundation. (a) 3 m in time domain; (b) 3 m in frequency domain; (c) 15 m in time domain; (d) 15 m in frequency domain; (e) 30 m in time domain; (f) 30 m in frequency domain; (g) 50 m in time domain; (h) 50 m in frequency domain.

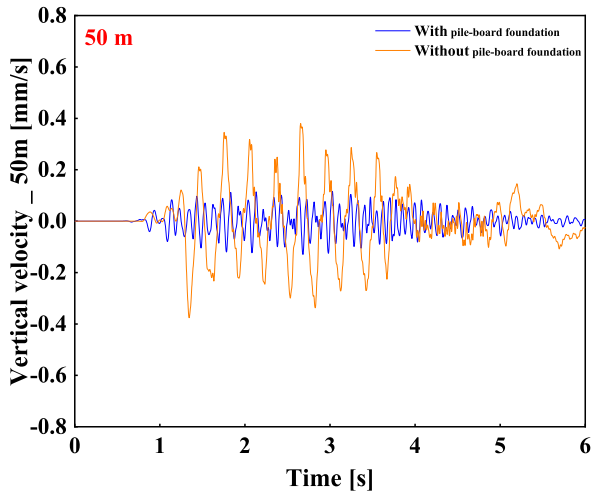

(g) 50 m in time domain

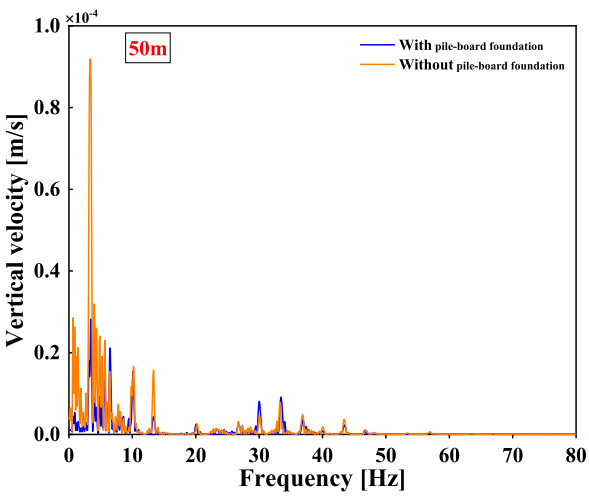

(h) 50 m in frequency domain

Fig. 10. (*continued*).

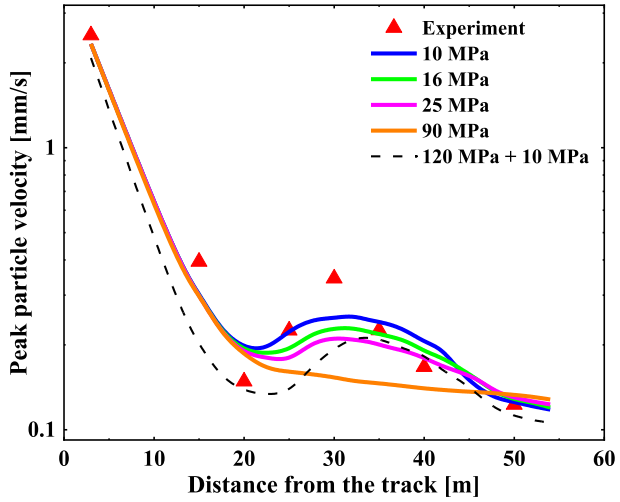

Fig. 11. Variation of vertical PPV with distance in terms of different Young's modulus of the natural soft soil.

It can be seen in Fig. 8 that the magnitudes are all quite similar between the responses to the 16-carriage trains and the 8-carriage trains. The soil responses induced by a 16-carriage train just lasted longer in time than that of an 8-carriage train.

Fig. 9 further compares the soil responses at 3 m with vehicle numbers from 1 to 16.

In Fig. 9(a), the soil responses at 3 m induced by various number of vehicles are extracted from the soil response of a typical 16-carriage train according to the visible passing wheelsets. It can be seen from Fig. 9(b) that, with more vehicles, the spectral peaks get narrower and more prominent. While with fewer vehicles, the spectral peaks become broader. When there is only one vehicle, the spectral peaks are round, and the vehicle passing frequency is not the same as that of the soil responses induced by 8 or more vehicles, as shown in the inset of Fig. 9 (b). Too few vehicles cannot make the spectral peaks as the integral multiples of the vehicle passing frequency.

The spectral peaks with 8 vehicles are almost identical to those with 16 vehicles both in magnitude and shape, thus the soil responses of an 8-carriage train is representative for that of a 16-carriage train in this research.

Influence of pile-board foundation

The influence of the pile-board foundation on the ground vibration is investigated by comparing the simulation results with and without the pile-board foundation. In the condition without the pile-board foundation, the space of the pile-board foundation is replaced by the construction-influenced soil. The comparison is shown in Fig. 10.

It can be seen from Fig. 10 that, if there is no pile-board foundation, the ground vibration will be considerably larger. At the embankment shoulder (see Fig. 10(a)), the vertical vibration velocity has increased about 30% when the pile-board foundation is missing. While at the place 15 m away from the track, instability appears when the train approaches and leaves the main part of the model, as shown in Fig. 10(c). This is probably because the ground stiffness is too low for a high speed train's passing-by when the substructure has no pile-board foundation. The pile-board foundation is able to improve the ground stiffness and make the substructure stronger with higher loadbearing capacity.

From Fig. 10(b), (d), (f) and (h), it can be seen that, the enlarged ground vibration is mainly contributed from the low frequency contents below 15 Hz. This is possibly because the pile-board foundation has the ability to introduce the vibration and waves into deeper ground soil, especially the waves with low frequencies. Then much more soil participates in the vibration and more soil damping takes effect, thus to more significantly attenuate the ground vibration. While for the high frequency contents, due to their short wavelengths and travelling along the shallow ground surface, the influence of the pile-board foundation is relatively small. It is worth mentioning that, when there is no pile-board foundation, the spectral peaks are still almost all at the integral multiples of the vehicle passing frequency.

Local vibration amplification

The amplification of seismic waves at a specific site may involve many factors, such as local geometric conditions, soil layer thickness, soil mechanical properties, impedance contrast between different soils [47–51]. Train-induced ground vibration propagates as waves. Thus, the vibration amplification at 30 m in this experiment is possibly related to some of these factors.

In the trail simulations, it is found that one of the most important influential factors on the local vibration amplification at 30 m is the Young's modulus of the natural soft soil. In Fig. 11, the influence of the Young's modulus of the natural soft soil on the amplification of the vertical PPV is investigated.

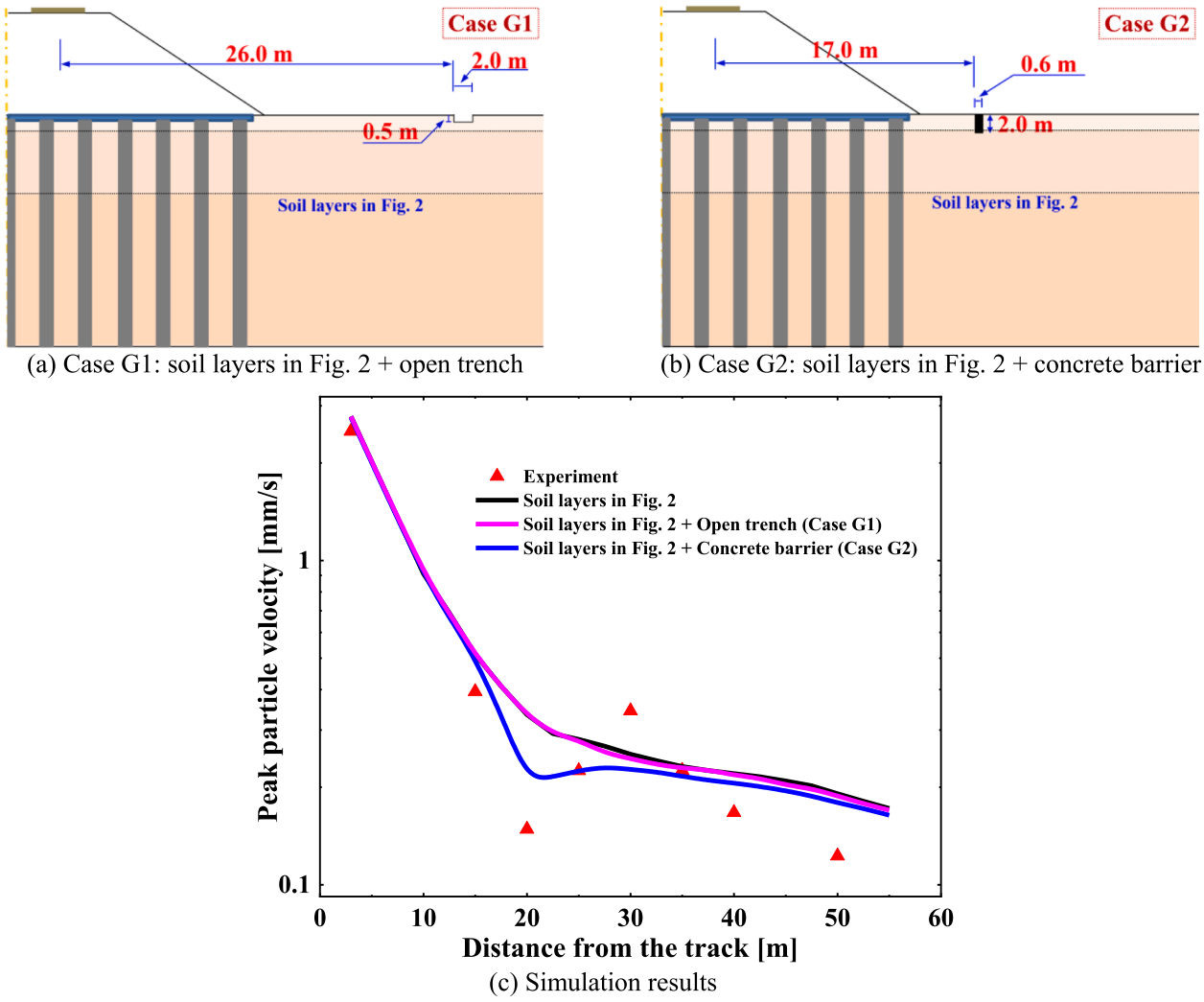

Fig. 12. Variation of vertical PPV with distance in terms of soil stratification and geometric discontinuity.

As shown in Fig. 11, the Young's modulus of the natural soft soil is varied from 10 MPa to 90 MPa (see the solid lines) while the other parameters in Section 4.1 are unchanged. The case of '90 MPa' in Fig. 11 means that the ground soil above the weathered amphibolite layer is homogenous. It can be seen from Fig. 11 that the softer natural soil, the larger the local amplification.

Another case considered in Fig. 11, as shown with the black dash line, is a combination of 120 MPa and 10 MPa for the Young's modulus of the construction-influenced soil and the Young's modulus of the natural soft soil, respectively. In this case, the impedance contrast between the construction-influenced soil and the natural soft soil is larger than that of the other cases. It looks that this case is not offering a better simulation result, but it indicates that larger soil impedance contrast makes larger vibration amplification.

When the Young's modulus of the natural soft soil is lower than 10 MPa, the local amplification can be even larger. To simulate wave propagation in soil with lower modulus will need finer mesh which requires a much larger number of elements, demanding higher computational cost.

Soil stratification causes ground vibration amplification in the usual sense. For that, many trial simulations were performed with the soil being considered consisting of multiple layers, for both the natural and construction-influenced soils. The layer thickness and material properties were varied. No significant effects of the layers were observed on the amplification. One such case is shown with the black solid line in Fig. 12(c), with the soil layer dimensions and soil properties shown in Fig. 2. It indicates that soil stratification is not the main cause of the local vibration amplification in this experiment.

It worth mentioning that, there is a shallow trench (less than 0.5 m in depth) at about 27 m and a concrete barrier at about 17 m away from the track, as shown in Fig. 1. These geometric discontinuities can also affect the ground vibration. An open trench has long been considered as a mitigation measure for ground vibration [52,53]. Thompson, *et al.* [54] investigated the effectiveness of an open trench by using a 2.5D FE-BE method. It concluded that, a trench works as a wave barrier and the depth is the most important parameter while the width has a small influence. Dijckmans, *et al.* [55] investigated the effectiveness of a sheet pile wall in soft soil on the railway induced ground vibration, and it found that, the efficacy of a stiff wave barrier is determined by the depth and the stiffness contrast with soil. Thus, extensive trial simulations were also performed, considering a trench and a stiff barrier, with a broad range of depth and width, as well as material properties. Indeed increasingly obvious effects of the trench and the stiff barrier on the amplification were observed with the increasing depth, but the effects were negligible when the depth was less than 0.5 m. An example is shown with Case G1 in Fig. 12. The dimensions and the position of the open trench is illustrated in Fig. 12(a) and the simulation result is shown with the pink solid line in Fig. 12(c). The shallow trench has negligible effect on the ground vibration. Another example is about the concrete barrier, as shown with the Case G2 in Fig. 12(b). It can be seen from the

blue solid line in Fig. 12(c) that, the concrete barrier with a depth of 2 m imposes an apparent reduction on the ground vibration at behind the barrier, and also has negative effect on the ground vibration at locations from 25 to 40 m. In addition, the concrete barrier is usually very shallow and its actual depth is even less than 0.5 m. Therefore, neither the shallow trench nor the concrete barrier is the main cause of the local vibration amplification in this experiment.

In the future, the proposed model will be employed to investigate the influences of various factors, such as track irregularities, varying soil properties and the associated nonlinearities [56], and especially the transition zone between the construction-influenced soil and the natural soft soil, so as to facilitate the development of vibration isolation and attenuation methods.

Conclusions and future work

In this work, an explicit time-domain, fully coupled 3D dynamic train-track-embankment-piles-soil FE model is developed and validated with in situ experimental results. Good agreements between numerical and experimental results have been achieved both in time domain and frequency domain. The dynamic ground responses induced by a typical high speed train have been successfully simulated.

The soil responses induced by different number of vehicles in a train are compared. It is demonstrated that with more vehicles, the spectral peaks of the responses are more prominent at integral multiples of the vehicle passing frequency. Too few vehicles will not bring about such phenomenon thus sufficient number of vehicles should be included in a train to properly model train-induced ground vibration. It is shown that 8 vehicles, each with 4 axles, are enough for such a purpose.

The influence of the pile-board foundation on the ground vibration is investigated. It is found that the pile-board foundation can significantly attenuate the ground vibration, especially the low frequency contents. It is probably because the pile-board foundation can improve the ground stiffness and also introduce the propagating waves into deeper ground soil thus more soil damping takes effect.

In the experiment, at the place about 30 m from the track, the soil surface vibration was amplified. With the proposed model, efforts are made to identify the factors influential to the local vibration amplification. It is found that the softer natural soil, the larger amplification. Larger soil impedance contrast makes the amplification more obvious. The soil stratification and geometric discontinuity at ground surface, which are the causes of local vibration amplification in the usual sense, are not the main cause in this work.

Further study is needed to gain more insight into the factors that determine the local vibration amplification. The model can then be used for better understanding of train-induced ground vibration, so as to design effective isolation and attenuation methods.

Declaration of Competing Interest

The authors declare that they have no known competing financial interests or personal relationships that could have appeared to influence the work reported in this paper.

Acknowledgements

The authors would like to thank the anonymous reviewers for their critical and constructive comments. The helpful suggestions and comments of Dr. Alfredo Núñez Vicencio are gratefully acknowledged.

References

[1] Thompson DJ, Kouroussis G, Ntotsios E. Modelling, simulation and evaluation of ground vibration caused by rail vehicles. Veh Syst Dyn 2019;57(7):936–83.
[2] Sheng X. A review on modelling ground vibrations generated by underground trains. Int J Rail Transp 2019;7(4):241–61.
[3] Connolly DP, Marecki GP, Kouroussis G, Thalassinakis I, Woodward PK. The growth of railway ground vibration problems - a review. Sci Total Environ 2016;568:1276–82.
[4] Degrande G, Schillemans L. Free field vibrations during the passage of a Thalys high-speed train at variable speed. J Sound Vib 2001;247(1):131–44.
[5] Lombaert G, Degrande G. Ground-borne vibration due to static and dynamic axle loads of InterCity and high-speed trains. J Sound Vib 2009;319(3-5):1036–66.
[6] Galvín P, Domínguez J. Experimental and numerical analyses of vibrations induced by high-speed trains on the Córdoba-Málaga line. Soil Dyn Earthquake Eng 2009;29(4):641–57.
[7] Zhang X, Zhou S, He C, Di H, Si J. Experimental investigation on train-induced vibration of the ground railway embankment and under-crossing subway tunnels. Transp Geotech 2021;26:100422. https://doi.org/10.1016/j.trgeo.2020.100422.
[8] Auersch L. Wave Propagation in Layered Soils: Theoretical Solution in Wavenumber Domain and Experimental Results of Hammer and Railway Traffic Excitation. J Sound Vib 1994;173(2):233–64.
[9] Krylov V, Ferguson C. Calculation of low-frequency ground vibrations from railway trains. Appl Acoust 1994;42(3):199–213.
[10] Krylov VV. Generation of ground vibrations by superfast trains. Appl Acoust 1995;44(2):149–64.
[11] Krylov V. Effect of track properties on ground vibrations generated by high speed trains. Acustica-Acta Acustica 1998;84(1):78–90.
[12] Ford RAJ. Track and ground vibrations from trains running on conventional ballasted track. Proc Instit Mech Eng Part F: J Rail Rapid Trans 1992;206(2):117–26.
[13] Jones CJC, Block JR. Prediction of ground vibration from freight trains. J Sound Vib 1996;193(1):205–13.
[14] Yang YB, Hung HHA. 2.5D finite/infinite element approach for modelling visco-elastic bodies subjected to moving loads. Int J Numer Meth Eng 2001;51(11):1317–36.
[15] Yang YB, Hung HH, Chang DW. Train-induced wave propagation in layered soils using finite/infinite element simulation. Soil Dyn Earthquake Eng 2003;23(4):263–78.
[16] Jean P, Guigou C, Villot M. A 2.5D BEM Model for Ground-Structure Interaction. Build Acoust 2004;11(3):157–73.
[17] Sheng X, Jones CJC, Thompson DJ. Modelling ground vibration from railways using wavenumber finite- and boundary-element methods. Proc Roy Soc A 2005;461(2059):2043–70.
[18] Sheng X, Jones CJC, Thompson DJ. Prediction of ground vibration from trains using the wavenumber finite and boundary element methods. J Sound Vib 2006;293(3-5):575–86.
[19] Degrande G, Clouteau D, Othman R, Arnst M, Chebli H, Klein R, et al. A numerical model for ground-borne vibrations from underground railway traffic based on a periodic finite element-boundary element formulation. J Sound Vib 2006;293(3-5):645–66.
[20] Gupta S, Van den Berghe H, Lombaert G, Degrande G. Numerical modelling of vibrations from a Thalys high speed train in the Groene Hart tunnel. Soil Dyn Earthquake Eng 2010;30(3):82–97.
[21] Ju S-H, Lin H-T. Analysis of train-induced vibrations and vibration reduction schemes above and below critical Rayleigh speeds by finite element method. Soil Dyn Earthquake Eng 2004;24(12):993–1002.
[22] Galvín P, Romero A, Domínguez J. Fully three-dimensional analysis of high-speed train–track–soil-structure dynamic interaction. J Sound Vib 2010;329(24):5147–63.
[23] Kouroussis G, Verlinden O, Conti C. Free field vibrations caused by high-speed lines: Measurement and time domain simulation. Soil Dyn Earthquake Eng 2011;31(4):692–707.
[24] Kouroussis G, Verlinden O, Conti C. Influence of some vehicle and track parameters on the environmental vibrations induced by railway traffic. Veh Syst Dyn 2012;50(4):619–39.
[25] Kouroussis G, Conti C, Verlinden O. Investigating the influence of soil properties on railway traffic vibration using a numerical model. Veh Syst Dyn 2013;51(3):421–42.
[26] Connolly D, Giannopoulos A, Forde MC. Numerical modelling of ground borne vibrations from high speed rail lines on embankments. Soil Dyn Earthquake Eng 2013;46:13–9.
[27] Li T, Su Q, Kaewunruen S. Saturated ground vibration analysis based on a Three-Dimensional coupled Train-Track-Soil interaction model. Appl Sci 2019;9(23):4991.
[28] Li T, Su Q, Kaewunruen S. Influences of piles on the ground vibration considering the train-track-soil dynamic interactions. Comput Geotech 2020;120:103455. https://doi.org/10.1016/j.compgeo.2020.103455.
[29] Auersch L. The excitation of ground vibration by rail traffic: theory of vehicle-track-soil interaction and measurements on high-speed lines. J Sound Vib 2005;284(1-2):103–32.
[30] Zhai WM, Wei K, Song XL, Shao MH. Experimental investigation into ground vibrations induced by very high speed trains on a non-ballasted track. Soil Dyn Earthquake Eng 2015;72:24–36. https://doi.org/10.1016/j.soildyn.2015.02.002.
[31] Feng S-J, Zhang X-L, Wang L, Zheng Q-T, Du F-L, Wang Z-L. In situ experimental study on high speed train induced ground vibrations with the ballast-less track. Soil Dyn Earthquake Eng 2017;102:195–214.
[32] Wang P, Wei K, Wang Li, Xiao J. Experimental study of the frequency-domain characteristics of ground vibrations caused by a high-speed train running on non-ballasted track. Proc Instit Mech Eng, Part F: J Rail Rapid Trans 2016;230(4):1131–44.
[33] Code for design of railway earth structure. TB 10001-2016 [In Chinese].

[34] Lei X, Wang J. Dynamic analysis of the train and slab track coupling system with finite elements in a moving frame of reference. J Vib Control 2014;20(9):1301–17.
[35] Zhai WM. Vehicle – track coupled dynamics: theory and applications. Singapore: Springer; 2020. p. 183–96.
[36] Munich Research Center of German Federal Railway. ICE technology assignment for inter-city express train; 1993.
[37] Garg VK, Dukkipati RV. Dynamics of railway vehicle systems. Ontario: Academic Press, Canada; 1984.
[38] PSD of ballastless track irregularities of high speed railway. TB/T 3352-2014 [In Chinese].
[39] Luo Q, Wei M, Lu Q, Wang T. Simplified analytical solution for stress concentration ratio of piled embankments incorporating pile-soil interaction. Railw Eng Sci 2021; 29(2):199–210.
[40] Basu U. Explicit finite element perfectly matched layer for transient three-dimensional elastic waves. Int J Numer Meth Eng 2009;77(2):151–76.
[41] Semblat J-F, Gandomzadeh A, Lenti L. A simple numerical absorbing layer method in elastodynamics. CR Mec 2010;338(1):24–32.
[42] Kouroussis G, Verlinden O, Conti C. Finite-dynamic model for infinite media: corrected solution of viscous boundary efficiency. J Eng Mech 2011;137(7): 509–11.
[43] Deutsches Institut für Normung. DIN4150-2: Structural vibrations-Part 2: Human exposure to vibration in buildings; 1999.
[44] Xia H, Zhang N, Cao YM. Experimental study of train-induced vibrations of environments and buildings. J Sound Vib 2005;280(3-5):1017–29.
[45] Milne DRM, Le Pen LM, Thompson DJ, Powrie W. Properties of train load frequencies and their applications. J Sound Vib 2017;397:123–40.
[46] Le Pen L, Milne D, Thompson D, Powrie W. Evaluating railway track support stiffness from trackside measurements in the absence of wheel load data. Can Geotech J 2016;53(7):1156–66.
[47] Semblat JF, Kham M, Parara E, Bard PY, Pitilakis K, Makra K, et al. Seismic wave amplification: Basin geometry vs soil layering. Soil Dyn Earthquake Eng 2005;25 (7-10):529–38.
[48] Baise LG, Kaklamanos J, Berry BM, Thompson EM. Soil amplification with a strong impedance contrast: Boston, Massachusetts. Eng Geol 2016;202:1–13.
[49] Narayan JP. Effects of impedance contrast and soil thickness on basin-transduced Rayleigh waves and associate differential ground motion. Pure Appl Geophys 2010; 167:1485–510.
[50] Bazzurro P, Cornell CA. Ground motion amplification in nonlinear soil sites with uncertain properties. Bull Seismol Soc Am 2004;94(6):2090–109.
[51] Wang Z, Nagashima F, Kawase H. A new empirical method for obtaining horizontal site amplification factors with soil nonlinearity. Earthq Eng Struct Dyn 2021;50 (10):2774–94.
[52] Woods RD. Screening of Surface Wave in Soils. J Soil Mech Found Div, ASCE 1968; 94(4):951–79.
[53] Alzawi A, Hesham El Naggar M. Full scale experimental study on vibration scattering using open and in-filled (GeoFoam) wave barriers. Soil Dyn Earthquake Eng 2011;31(3):306–17.
[54] Thompson DJ, Jiang J, Toward MGR, Hussein MFM, Ntotsios E, Dijckmans A, et al. Reducing railway-induced ground-borne vibration by using open trenches and soft-filled barriers. Soil Dyn Earthquake Eng 2016;88:45–59.
[55] Dijckmans A, Ekblad A, Smekal A, Degrande G, Lombaert G. Efficacy of a sheet pile wall as a wave barrier for railway induced ground vibration. Soil Dyn Earthquake Eng 2016;84:55–69.
[56] Shih JY, Thompson DJ, Zervos A. The influence of soil nonlinear properties on the track/ground vibration induced by trains running on soft ground. Transp Geotech 2017;11:1–16. https://doi.org/10.1016/j.trgeo.2017.03.001.